

Construction of full-color-tunable and strongly emissive materials by functionalizing a boron-chelate four-ring-fused π -conjugated core†

Di Li, Hongyu Zhang,* Chenguang Wang, Shuo Huang, Jianhua Guo and Yue Wang*

Received 16th September 2011, Accepted 9th November 2011

DOI: 10.1039/c1jm14606h

2-(2'-Hydroxyphenyl)benzoxazole (HBO) and 2-(2'-hydroxyphenyl)benzothiazole (HBT) reacted with triphenylborane produced two rigid π -conjugated fluorescent cores **1** (BPh₂(BOZ), BOZ = 2-(benzo[d]oxazol-2-yl)phenol) and **2** (BPh₂(BTZ), BTZ = 2-(benzo[d]thiazol-2-yl)phenol). Comparisons of photophysical properties and calculations between *para*- and *meta*-diphenylamine-substituted derivatives **5** (BPh₂(*para*-NPh₂-BTZ)) and **7** (BPh₂(*meta*-NPh₂-BTZ)) demonstrated that functionalization at the *para*-position of the rigid core is effective in tuning the electronic structure and hence the photophysical properties of this type of boron-chelate complex. Simple modification of these frameworks by introducing various amine groups at the *para*-position allows the synthesis of strongly fluorescent materials **3** (BPh₂(*para*-Cz-BTZ), Cz = 9*H*-carbazol-9-yl), **4** (BPh₂(*para*-NPh₂-BOZ), NPh₂ = diphenylamino), **5**, and **6** (BPh₂(*para*-NMe₂-BTZ), NMe₂ = dimethylamino). The emission colors of these newly synthesized complexes together with the parent complexes **1** and **2** covered a wide range from deep blue to saturated red in both solution and the solid state. Crystal structure analysis discloses that two phenyl groups attached to the boron atom effectively keep the luminescent ring-fused π -conjugated skeletons apart, making these fluorophores highly emissive in solid forms ($\Phi_F = 0.36\text{--}0.71$). Organic light-emitting diodes employing these boron complexes as emitters not only keep the full-color tunable emission feature but also show high electroluminescent (EL) performance; for instance, the greenish-blue device based on **2** showed the highest efficiency of 7.8 cd A⁻¹ and the yellow light-emitting device based on **4** exhibited the highest brightness (31 220 cd m⁻²) among the boron-containing emitters reported so far.

Introduction

The development of highly emissive organic materials in the solid state is a fundamental and important requirement for various optoelectronic applications, such as organic light-emitting diodes (OLEDs), organic lasers, and sensors.¹ In the construction of emitting materials, tunable emission color and high solid-state quantum efficiency are two important issues in terms of optoelectronic applications of materials. To realize the effective color tuning, many strategies including copolymerization have been empirically pursued, there exists only a limited number of emissive core skeletons with flexibility in their synthetic strategies for tunable emission wavelengths.^{1a,2} In this regard, it is urgently demanded to develop fluorescent cores with flexibility in structural functionalization for full-color fluorescence. As for the

fluorescence efficiency, whereas a lot of fluorophores emit strongly when molecularly dissolved in solvents, they become weak fluorophores in the solid state due to either attractive dipole-dipole interactions or intermolecular π -stacking.³ Considering that the fluorescent materials are used as solid forms in most applications, how to suppress the quenching process is thus highly important.

Extended π -conjugated molecules with ring-fused structures have attracted considerable attention since their structural feature of flat and rigid π -conjugated skeletons bring about a set of desired properties such as intense luminescence, good thermal stability and high carrier mobility.⁴ Introducing main group elements, such as nitrogen, silicon, sulfur, selenium, boron, and phosphorus into this type of π -plane have proved to be an efficient way to modulate their optoelectronic properties.⁵ In particular, incorporation of four-coordinate boron moieties into the extended π -conjugated framework might be of interest considering that four-coordinate boron complexes have wide applications in OLEDs.^{6,7} Along this line of consideration, we have recently synthesized several series of brightly fluorescent solids by incorporation of four-coordinate boron moieties into the extended π -conjugated skeletons and found that these

State Key Laboratory of Supramolecular Structure and Materials, College of Chemistry, Jilin University, Changchun, 130012, P. R. China. E-mail: hongyuzhang@jlu.edu.cn; yuewang@jlu.edu.cn; Tel: +86-431-85168484

† Electronic supplementary information (ESI) available: Theoretical calculations, electrochemical spectra, DSC and TGA curves. CCDC reference numbers 837275–837277. For ESI and crystallographic data in CIF or other electronic format see DOI: 10.1039/c1jm14606h

molecules could serve as efficient emitters in OLEDs with an intrinsic electron-transporting nature.⁸ Modulating the length of the core skeletons, such as in five-, six-, and seven-ring-fused systems, significantly affects the emission color of the produced molecules, and altering the bridging atoms of frameworks or substitutes on the boron atoms can further tune their fluorescence. While these synthetic strategies allowed the construction of a family of boron-containing emitting materials with fluorescence covering a wide range from pure blue (450 nm) to saturated red (670 nm), from a viewpoint of simplifying the synthetic procedure, it is strikingly attractive to develop a rigid boron-chelate fluorescent core that has flexibility in structural modulation for color tuning.

Recently, Kwak and Kim reported two BF₂-chelate fluorophores based on 2-(2'-hydroxyphenyl)benzoxazole (HBO) and 2-(2'-hydroxyphenyl)benzothiazole (HBT) ligands that emit blue fluorescence with moderate quantum yields ($\Phi_F = 0.20$ and 0.23) in solution.⁹ Employing HBO and HBT ligands, we have synthesized two BPh₂-chelate analogs **1** and **2** and found these boron complexes having four-ring-fused core skeleton together with bulky side aryl groups emit very bright blue or cyan fluorescence in both solution ($\Phi_F = 0.55$ for **1** and 0.65 for **2**) and the solid state ($\Phi_F = 0.53$ for **1** and 0.60 for **2**).^{8d} In addition, our recent findings disclosed that the electronic structures of the precursor ligands could be effectively tuned by a *para*-substitution with various amine groups.¹⁰ In view of these results, it appeared attractive to attempt *para*-modification of the fluorescent BPh₂-chelate four-ring-fused skeleton with an aim to construct materials with tunable emission colors and high fluorescence efficiencies. Indeed, a simple functionalization of this type of boron-bridged fluorescent core by introducing amine groups with varying electron-donating ability (Chart 1) allows us to synthesize a series of strongly fluorescent materials **3–6** which together with the parents **1** and **2** exhibit emission colors ranging from deep blue to saturated red. The substitution position effect was investigated by a comparison of photophysical properties between *para*- and *meta*-diphenylamine-substituted complexes **5** and **7**. Fundamental properties of the newly synthesized complexes **3–6** together with the parent BPh₂-chelate complexes **1** and **2** were fully demonstrated. To test the possibility of this

kind of boron complexes as emitting materials in OLEDs, electroluminescent (EL) devices employing **1–6** as emitters have also been fabricated and characterized.

Experimental

General information

All starting materials were purchased from Aldrich Chemical Co. and used without further purification. The solvents for syntheses were freshly distilled over appropriate drying reagents. All experiments were performed under a nitrogen atmosphere using standard Schlenk techniques. ¹H NMR spectra were measured on a Bruker AVANCE 300 or 500 MHz spectrometer with tetramethylsilane as the internal standard. Mass spectra were recorded on a Shimadzu AXIMA-CFR MALDI-TOF mass spectrometer. Elemental analyses were performed on a flash EA 1112 spectrometer. UV-vis absorption spectra were recorded using a PE UV-vis lambdaDazo spectrometer. The emission spectra were recorded using a Maya2000 Pro CCD spectrometer. Electrochemical measurements were performed with a BAS 100W Bioanalytical electrochemical work station. Differential scanning calorimetric (DSC) measurements were performed on a NETZSCH DSC204 instrument. Thermogravimetric analyses (TGA) were performed on a TA Q500 thermogravimeter. 2-(Benzo[d]thiazol-2-yl)-4-(9*H*-carbazol-9-yl)phenol (**HL3**), 2-(benzo[d]oxazol-2-yl)-4-(diphenylamino)phenol (**HL4**), 2-(benzo[d]thiazol-2-yl)-4-(diphenylamino)phenol (**HL5**), 2-(benzo[d]thiazol-2-yl)-4-(dimethylamino)phenol (**HL6**) and 2-(benzo[d]thiazol-2-yl)-5-(diphenylamino)phenol (**HL7**) were synthesized according to the literature procedures.¹⁰

General synthetic procedure

To a rapidly stirred solution of ligand in THF, 1.1 mol of BPh₃ in THF was added and the mixture was stirred overnight at room temperature. The volatiles were removed under vacuum, and the residual solid was purified by vacuum sublimation to give the boron complex as a solid.

Complex 3. Yield was 52% as green powder. ¹H NMR (CDCl₃, 500 MHz, ppm): δ 8.15 (d, $J = 8.0$ Hz, 2 H), 7.87 (d, $J = 8.0$ Hz, 1 H), 7.72 (d, $J = 2.5$ Hz, 1 H), 7.62 (dd, $J = 8.5$ Hz, 2.5 Hz, 1 H), 7.45–7.27 (m, 20 H). MS m/z : 556.6 [M]⁺ (calcd: 556.2). Anal. Calcd (%) for C₃₇H₂₅BN₂OS: C, 79.86; H, 4.53; N, 5.03; S, 5.76; Found: C, 79.56; H, 4.42; N, 5.02; S, 5.65.

Complex 4. Yield was 46% as yellow powder. ¹H NMR (CDCl₃, 500 MHz, ppm): δ 7.58 (d, $J = 8.0$ Hz, 1 H), 7.54 (d, $J = 3.0$ Hz, 1 H), 7.46–7.44 (m, 4 H), 7.39 (t, $J = 7.5$ Hz, 1 H), 7.35 (dd, $J = 9.0$ Hz, 2.5 Hz, 1 H), 7.27–7.24 (m, 11 H), 7.14 (d, $J = 9.0$ Hz, 1 H), 7.08 (d, $J = 8.0$ Hz, 4 H), 7.02–6.99 (m, 3 H). MS m/z : 542.2 [M]⁺ (calcd: 542.2). Anal. Calcd (%) for C₃₇H₂₇BN₂O₂: C, 81.93; H, 5.02; N, 5.16; Found: C, 81.81; H, 4.93; N, 5.15.

Complex 5. Yield was 59% as orange powder. ¹H NMR (CDCl₃, 500 MHz, ppm): δ 7.79 (d, $J = 8.0$ Hz, 1 H), 7.39–7.36 (m, 5 H), 7.30–7.23 (m, 14 H), 7.11–7.06 (m, 5 H), 7.00 (t, $J = 7.5$ Hz, 2 H). MS m/z : 558.6 [M]⁺ (calcd: 558.2). Anal. Calcd (%) for

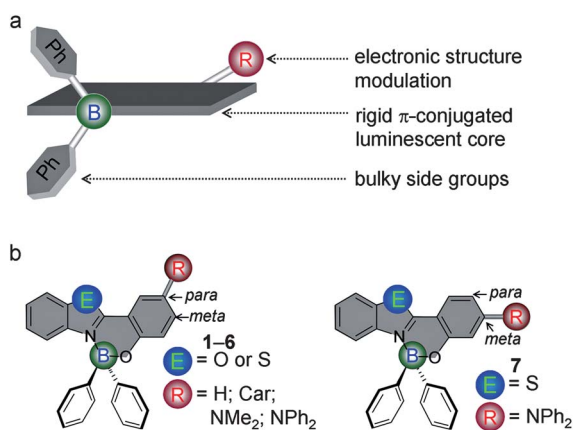


Chart 1 (a) Structural feature of boron-chelate four-ring-fused electron-system and (b) derivation of the core skeleton at the *para*- or *meta*-position.

$C_{37}H_{27}BN_2OS$: C, 79.57; H, 4.87; N, 5.02; S, 5.74; Found: C, 79.28; H, 4.70; N, 4.95; S, 5.64.

Complex 6. Yield was 40% as red powder. 1H NMR ($CDCl_3$, 500 MHz, ppm): δ 7.84 (d, $J = 8.0$ Hz, 1 H), 7.40–7.36 (m, 5 H), 7.24–7.20 (m, 8 H), 7.13 (d, $J = 9.0$ Hz, 1 H), 7.08 (dd, $J = 9.0$ Hz, 2.5 Hz, 1 H), 6.71 (d, $J = 3.0$ Hz, 1 H), 2.88 (s, 6 H). MS m/z : 434.4 $[M]^+$ (calcd: 434.2). Anal. Calcd (%) for $C_{27}H_{23}BN_2OS$: C, 74.66; H, 5.34; N, 6.45; S, 7.38; Found: C, 74.74; H, 5.28; N, 6.50; S, 7.33.

Complex 7. Yield was 46% as yellow powder. 1H NMR (DMSO, 300 MHz, ppm): δ 8.20 (d, $J = 8.4$ Hz, 1 H), 7.57 (d, $J = 8.7$ Hz, 1 H), 7.46–7.38 (m, 5 H), 7.29–7.23 (m, 7 H), 7.16 (s, 10 H), 6.98 (d, $J = 8.4$ Hz, 1 H), 6.29 (dd, $J = 9.0$ Hz, $J = 2.4$ Hz, 1 H), 6.11 (d, $J = 2.4$ Hz, 1 H). MS m/z : 558.4 $[M]^+$ (calcd: 558.2). Anal. Calcd (%) for $C_{37}H_{27}BN_2OS$: C, 79.57; H, 4.87; N, 5.02; S, 5.74; Found: C, 79.61; H, 4.98; N, 5.16; S, 5.78.

X-Ray diffraction

Diffraction data were collected on a Rigaku RAXIS-PRID diffractometer using the ω -scan mode with graphite-monochromator Mo-K α radiation. The structures were solved with direct methods using the SHELXTL programs and refined with full-matrix least-squares on F^2 .¹² Non-hydrogen atoms were refined anisotropically. The positions of hydrogen atoms were calculated and refined isotropically. Crystallographic data (excluding structure factors) for the structure(s) reported in this paper have been deposited with the Cambridge Crystallographic Data Centre: CCDC 837275 for **1**, CCDC 837276 for **2**, and CCDC 837277 for **6**.†

Crystal data for 1. $C_{25}H_{18}BNO_2$, $M = 375.21$, monoclinic, $a = 26.232(5)$, $b = 10.000(2)$, $c = 15.213(3)$ Å, $U = 3923.4(13)$ Å³, $T = 293(2)$ K, space group $C2/c$, $Z = 8$, 14832 reflections measured, 3454 unique ($R_{int} = 0.1215$) which were used in all calculations. The final $wR(F^2)$ was 0.1540 (all data). *Crystal data for 2.* $C_{25}H_{18}BNOS$, $M = 391.27$, monoclinic, $a = 9.781(2)$, $b = 13.651(3)$, $c = 16.457(5)$ Å, $U = 2006.3(9)$ Å³, $T = 293(2)$ K, space group $P2_1/c$, $Z = 4$, 18861 reflections measured, 4559 unique ($R_{int} = 0.0678$) which were used in all calculations. The final $wR(F^2)$ was 0.1502 (all data). *Crystal data for 6.* $C_{27}H_{23}BN_2OS$, $M = 434.34$, monoclinic, $a = 13.017(3)$, $b = 12.930(3)$, $c = 18.193(6)$ Å, $U = 2256.9(10)$ Å³, $T = 293(2)$ K, space group $P2_1/c$, $Z = 4$, 21232 reflections measured, 5154 unique ($R_{int} = 0.0489$) which were used in all calculations. The final $wR(F^2)$ was 0.1137 (all data).

Theoretical calculations

The ground state geometries were fully optimized by the density functional theory (DFT)¹³ method with the Becke three-parameter hybrid exchange and the Lee–Yang–Parr correlation functional¹⁴ (B3LYP) and 6-31G* basis set using the Gaussian 03 software package.¹⁵

Fabrication of EL devices

Indium-tin oxide (ITO) coated glass was used as the substrate. It was cleaned by sonication successively in a detergent solution of acetone, methanol, and deionized water before use. The devices

were prepared in vacuum at a pressure of 5×10^{-6} Torr. Organic layers were deposited onto the substrate at a rate of 1–2 Å s⁻¹. After the organic film deposition, LiF and aluminium were thermally evaporated onto the organic surface. The thicknesses of the organic materials and the cathode layers were controlled using a quartz crystal thickness monitor. The electrical characteristics of the devices were measured with a Keithley 2400 source meter. The EL spectra and luminance of the devices were obtained on a PR650 spectrometer. The *N,N'*-bis(naphthalen-1-yl)-*N,N'*-bisphenyl)-benzidine (NPB), 2,2',2''-(1,3,5-benzotriptyl)-tris(1-phenyl-1-H-benzimidazole) (TPBi), tris(8-hydroxyquinolino) aluminium (Alq₃) and bis(10-hydroxybenzo[h]quinolino) beryllium (Bebq₂) were purchased from Jilin Optical and Electronic Materials Corp.

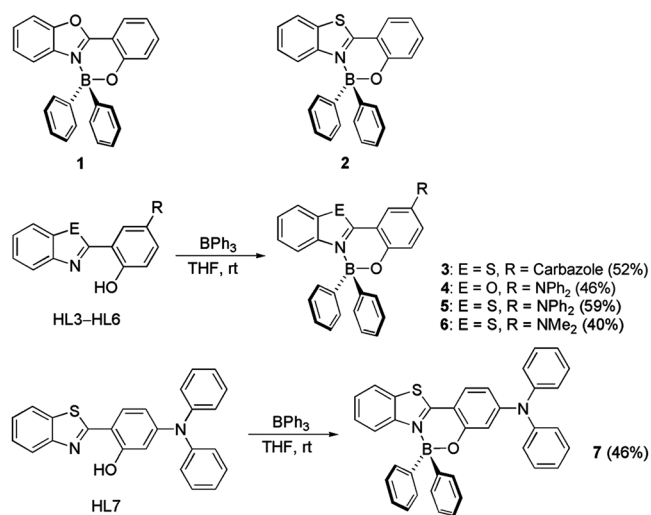
Results and discussion

Synthesis

The molecular structures of BPh₂-chelate parent complexes **1** and **2** and synthetic routes of amine-substituted complexes **3–6** are outlined in Scheme 1. The precursor ligands HL3–HL7 were synthesized following the reported literatures.¹⁰ Simple mixing of the ligands and triphenylborane in THF at room temperature and subsequent purification by vacuum sublimation produced targets **3–6** in moderate yields (40–59%). Boron complex **7** was synthesized by the same way in 46% yield for the purpose of defining the substitution position effect. All the newly synthesized boron complexes were fully characterized by 1H NMR, mass spectra, and elemental analyses.

Substitution position effect

To evaluate the substitution position (*para*- or *meta*-) effect on the photophysical properties, the absorption and emission spectra of diphenylamine-substituted boron complexes **5** and **7** in CH₂Cl₂ were compared. These two complexes showed completely different absorption and emission properties merely due to the subtle difference in substitution position, despite their



Scheme 1 Molecular structures of complexes **1** and **2** and synthetic routes for complexes **3–7**.

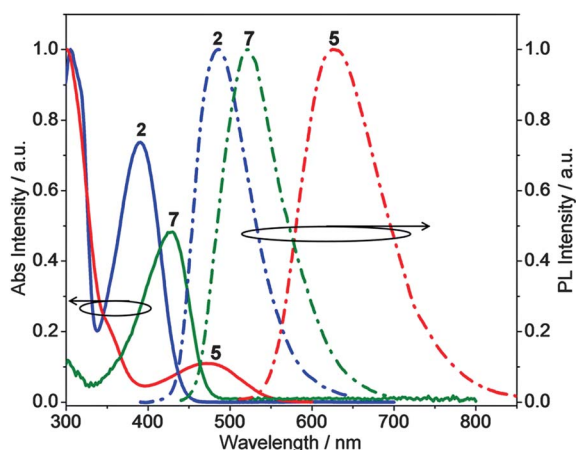


Fig. 1 Comparisons of absorption (solid line) and emission (dashed line) properties among complexes **2**, **5**, and **7**.

structural similarity. As depicted in Fig. 1, the non-substituted boron complex **2** is greenish-blue emissive with an absorption band centred at 389 nm and an emission band which peaked at 485 nm. *meta*-Diphenylamine-substituted boron complex **7** is green fluorescent with the longest absorption maximum of 428 nm and emission band centered at 520 nm, exhibiting 39 and 35 nm redshifts for absorption and emission maxima compared to **2**. Surprisingly, the same group substituted at the *para*-position significantly affected the photophysical properties of the produced boron complex **5** which showed red fluorescence ($\lambda_{\text{abs}} = 472$ nm; $\lambda_{\text{em}} = 627$ nm). Compared with **2**, the absorption and emission bands were red shifted by 83 and 142 nm, respectively. According to density functional theory (DFT) calculations, the electron-donating group substituted at the *para*-position significantly pushed the HOMO level up, hence narrowing the bandgap of the boron complex; whereas that substituted at the *meta*-position pushed up both the HOMO and LUMO levels and thus only weakly influenced the bandgap (Fig. S1†). In view of these comparisons, it is clear that only the slight difference in the chemical structure, *i.e.*, whether the amine group is attached to the *para*- or *meta*-position on the hydroxyphenyl ring, results in a significant difference in the photophysical properties. The calculation and experimental results demonstrate that derivation at the *para*-position is more effective in tuning the luminescent properties of the HBO- and HBT-chelate boron complexes. Therefore, we next focus the discussion on the properties of the parent and *para*-substituted boron complexes.

Crystal structures

Single crystals of complexes **1**, **2** and **6** were obtained by vacuum sublimation and their structures were determined by X-ray crystallography. All boron atoms adopt typical tetrahedral geometry to form *N,O*-chelate six-membered rings which contribute to constructing the four-ring-fused π -conjugated skeletons (Fig. 2a, c and e). In the molecular structures, the six-membered rings constructed by boron chelation take a chair conformation in which the oxygen and boron atoms deviate from the central phenyl plane by 0.60 Å and 0.04 Å for **1**, 0.54 Å and

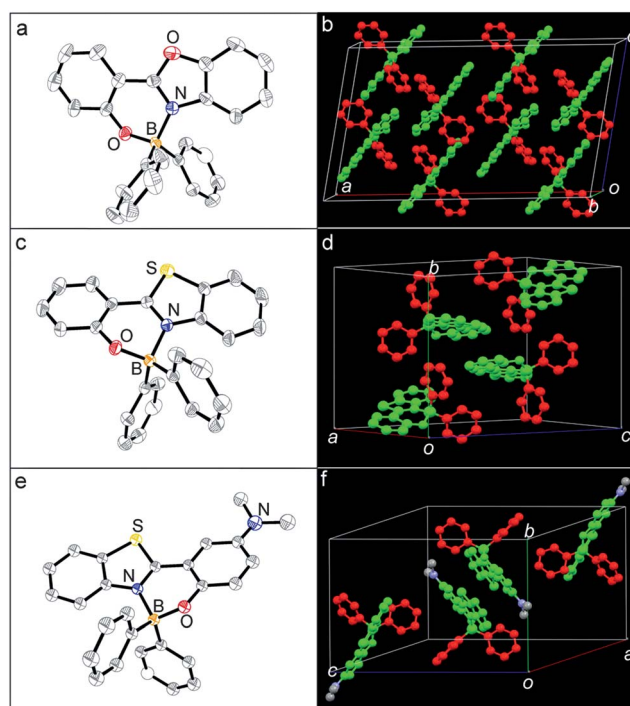


Fig. 2 Molecular structures of **1** (a), **2** (c), and **6** (e) with 50% thermal ellipsoids and packing structures of **1** (b), **2** (d), and **6** (f).

0.14 Å for **2**, and 0.51 Å and 0.11 Å for **6** in opposite directions. The bond lengths of B–O and B–N are 1.51 Å and 1.61 Å for **1**, 1.49 Å and 1.64 Å for **2**, and 1.49 Å and 1.65 Å for **6**, which are similar to those of the organoboron complexes reported previously.⁸ The dihedral angle between the outer benzene ring and the benzothiazole plane is 13.0° for **1**, 12.4° for **2**, and 10.6° for **6**, indicating that the four-ring-fused system has certain distortions from a coplanar framework.

Fig. 2b, d, f shows the molecular packing structures. The luminescent π -frameworks are effectively separated by two side phenyl rings attached to boron atoms; as a result, there are no π – π intermolecular interactions which usually exist in solids of

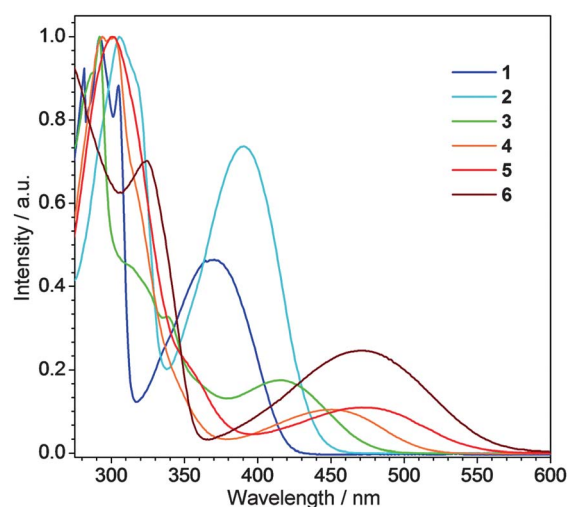


Fig. 3 Absorption spectra of complexes **1–6**.

Table 1 Photophysical data of complexes 1–6

Complex	$\lambda_{\text{abs}}/\text{nm}$	$\lambda_{\text{em}}/\text{nm}$ CH_2Cl_2^a	Stokes shift/nm	$\lambda_{\text{em}}/\text{nm}$ (solid)	Φ_{F} CH_2Cl_2^a	Φ_{F} (solid)
1	369	452	83	462	0.55	0.53
2	389	485	96	494	0.65	0.60
3	416	543	127	519	0.72	0.71
4	451	574	123	574	0.87	0.57
5	472	627	155	603	0.44	0.48
6	469	642	173	655	0.31	0.36

^a Concentration: 1.0×10^{-4} M.

fluorophores with an extended π -conjugated plane and results in severe fluorescence quenching. Such a molecular packing feature is important for luminescent fluorophores in maintaining a high fluorescent intensity in the solid state. This can not only explain why the BPh₂-chelate complexes **1** and **2** exhibit much higher quantum yields than the BF₂-chelate analogs in solution but also gives a possible explanation for the fact that complexes **1** and **2** keep quantum yields of their solutions and solids at a comparable level.

Photophysical properties

The absorption spectra of complexes **1–6** recorded in CH₂Cl₂ are shown in Fig. 3 and their data are summarized in Table 1. All of the complexes exhibited a broad absorption band ($\lambda_{\text{max}} = 369$ nm for **1**, 389 nm for **2**, 416 nm for **3**, 451 nm for **4**, 472 nm for **5**, and 469 nm for **6**) attributable to the electronic transition originating from the π -molecular orbitals. The amine derivatives **3–6** showed red-shifted absorption bands when compared to the non-substituted complexes **1** and **2**, reflecting the impact of the amine groups on the electronic properties. It is worthy of note that the absorption bands of these amine derivatives are related to the

donor strength, for instance, stronger electron-donating diphenylamine- and dimethylamine-substituted complexes **5** and **6** exhibited a 56 nm and 53 nm redshift, respectively, compared to carbazole-substituted **3**. Another notable feature of the present system is the bridging atom effect. The longest absorption maximum of B,O-bridged complex **1** was blue-shifted by about 20 nm compared to that of the B,S-bridged complex **2**, demonstrating that altering the bridging atom also affects the electronic structure of the four-ring-fused skeleton greatly. This viewpoint was further verified by the comparison of absorption bands between B,O-bridged complex **4** and B,S-bridged complex **5** whose molecular structures had the same diphenylamine substitution.

The fluorescence spectra of complexes **1–6** and their photograph images of samples irradiated by UV lamp ($\lambda_{\text{ex}} = 365$ nm) in both solution and the solid state were recorded and shown in Fig. 4. All the fluorophores exhibited intense emission in CH₂Cl₂ solutions (Fig. 4a) when excited at their absorption maxima. The emission profiles of these complexes in solution, having emission bands that peaked at 452 nm (**1**, deep blue), 485 nm (**2**, greenish blue), 543 nm (**3**, green), 574 nm (**4**, yellow), 627 nm (**5**, red), and 642 nm (**6**, deep red), covered a wide range from deep blue to saturated red, reflecting that the amine derivation at the *para*-position was indeed effective in tuning the emission color of this type of boron-chelate fluorophore. The amine-substituted complexes **3–6** showed significantly red-shifted emission peaks compared to the non-substituted complexes **1** and **2**, consistent with the trend observed in the absorption spectra. Similar to the observation in the absorption profiles, the emission peaks of B,S-bridged complexes **2** and **5** were red shifted by 33 and 53 nm compared to their B,O-bridged analogs **1** and **4**. The absolute fluorescence quantum yields (Φ_{F}) of solutions calculated using an integrating sphere were estimated to be 0.55 for **1**, 0.65 for **2**, 0.72 for **3**, 0.87 for **4**, 0.44 for **5**, and 0.31 for **6**.

The solid-state fluorescence spectra of these complexes in powder forms were measured and are shown in Fig. 4b. The fluorescence of the solid samples with emission peaks at 462 nm for **1**, 494 nm for **2**, 519 nm for **3**, 574 nm for **4**, 603 nm for **5**, and 655 nm for **6** also covered a wide range from blue to deep red and the emission bands of **1**, **2**, **4**, and **6** matched well with those in solutions. The emission maxima of complexes **3** and **5** were both blue shifted by about 24 nm compared with those of solution samples, which reflected crystallochromy effects. All the solid samples are intensely emissive ($\Phi_{\text{F}} = 0.53$ for **1**, 0.60 for **2**, 0.71 for **3**, 0.57 for **4**, 0.48 for **5**, and 0.36 for **6**, determined using an integrating sphere) and the fluorescence efficiencies are

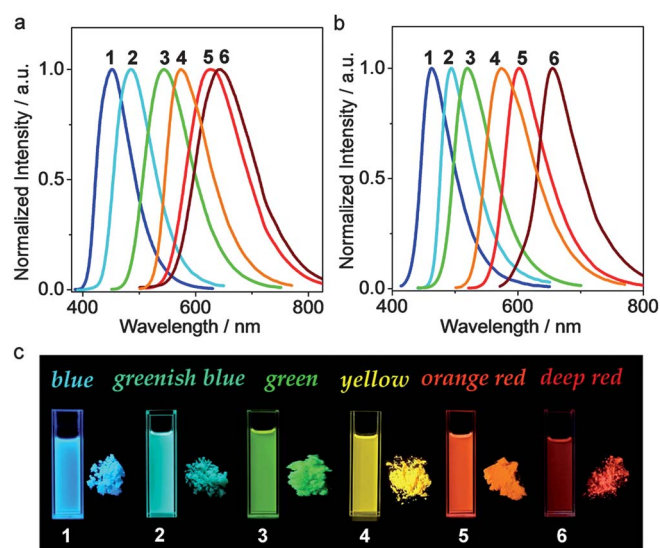


Fig. 4 Emission spectra (excited with longest absorption maxima) in CH₂Cl₂ (a), and the solid state (b), and photographic images (excited at 365 nm using a UV lamp) of solution and solid samples for complexes **1–6** (c).

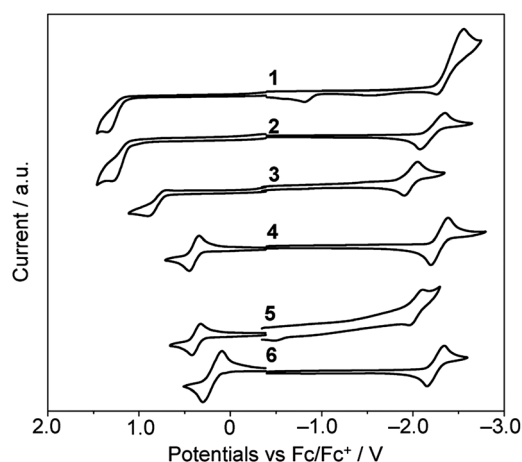


Fig. 5 Cyclic voltammograms of **1–6** in THF (reduction, 1 mM) and CH_2Cl_2 (oxidation, 1 mM), measured with TBAP (0.1 M) as a supporting electrolyte at a scan rate of 100 mV s^{-1} .

comparable to those of solutions. It is also worth noting that the solid-state quantum yields of **5** and **6** are at a very high level for materials with red or saturated red emissions. This is very important from the viewpoint of applying these complexes as emitting materials in OLEDs. The rigid core structure together with the bulky side phenyl groups attached to the boron atom play the major roles in maintaining the high fluorescence efficiencies from the solution phases to the solid forms.

Electrochemical properties

The electrochemical properties of these boron complexes **1–6** were characterized by cyclic voltammetry, and their cyclic voltammograms are shown in Fig. 5. The redox potentials are collected in Table 2.

All the complexes, except for **1**, exhibited a reversible cationic redox process corresponding to the reduction of the core skeleton. The half-wave potentials ($E_{\text{red}}^{1/2} = -2.28 \text{ V}$ for **1**, -2.21 V for **2**, -1.98 V for **3**, -2.29 V for **4**, -2.03 V for **5**, -2.25 V for **6**, vs. Fc/Fc^+) are very close to each other, indicating that the introduced amine segments do not greatly affect the electron affinity of the conjugated π -system. Complexes **2** and **5** showed slightly positively shifted reduction waves compared to complexes **1** and **4**, indicative of the certain enhancement of electron affinity when replacing the bridging oxygen atom by sulfur. On the basis of the reduction potentials, the lowest

unoccupied molecular orbital (LUMO) energy levels were calculated to be in the range of -2.51 to -2.82 eV .

Complexes **1** and **2** showed an irreversible anionic redox process with peak potentials at $+1.17$ and $+1.10 \text{ V}$, respectively, corresponding to oxidation of the conjugated core. The amine-substituted derivatives **4–6** displayed two reversible oxidation waves and their first oxidation potentials ($E_{\text{ox}}^{1/2} = +0.40 \text{ V}$ for **4**, $+0.37 \text{ V}$ for **5**, $+0.20 \text{ V}$ for **6**) were largely negatively shifted compared to non-substituted complexes **1** and **2**. Carbazole-substituted complex **3** exhibited the first quasi-reversible anionic redox process with an oxidation potential at $+0.73 \text{ V}$ which was also greatly negatively shifted compared to **2**. The significantly shifted oxidation potentials of the amine-substituted derivatives are considered to originate from the oxidation of amine groups. Diphenylamine- or dimethylamine-substituted complexes **4**, **5**, **6** showed lower oxidation potentials compared to **3**, due to their stronger electron-donating ability. The second oxidation processes of **3–6** had comparable onset potentials ($E_{\text{ox}}^{1/2} = +1.18 \text{ V}$ for **3**, $+1.02 \text{ V}$ for **4**, $+0.99 \text{ V}$ for **5**, $+0.90 \text{ V}$ for **6**) to those of **1** and **2**. These results mean that the second anionic redox process of complexes **3–6** corresponds to the oxidation of the core skeleton. Notably, in comparison with **1** and **2**, complexes **4**, **5**, and **6** have reversible second oxidation waves with slightly lower potentials; this is probably due to the presence of electron communication between the amine segment and the core skeleton which not only stabilizes the produced dication species but also enables the oxidation of the π -conjugated core

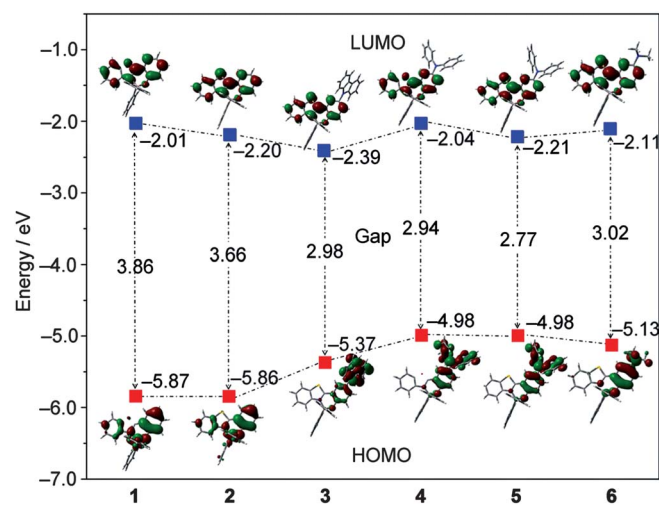


Fig. 6 Calculated molecular orbitals and energy levels of complexes **1–6**.

Table 2 Electrochemical and thermal data of complexes **1–6**^a

Complex	$E_{\text{ox}}^{1/2}/\text{V}$	$E_{\text{red}}^{1/2}/\text{V}$	HOMO/LUMO/Gap/ eV	$T_m/T_g/T_d^{5\%}/^\circ\text{C}$
1	+1.17/n.d.	-2.28	-5.97/-2.52/3.45	160/60/238
2	+1.10/n.d.	-2.21	-5.90/-2.59/3.31	211/75/264
3	+0.73/+1.18	-1.98	-5.53/-2.82/2.71	303/142/355
4	+0.40/+1.02	-2.29	-5.20/-2.51/2.69	n.d./105/324
5	+0.37/+0.99	-2.03	-5.17/-2.77/2.40	n.d./115/315
6	+0.20/+0.90	-2.25	-5.00/-2.55/2.45	269/129/306

^a n.d. = not observed.

more easily. On the basis of the first oxidation potentials, the highest occupied molecular orbital (HOMO) energy levels were calculated to be in the range of -5.00 to -5.97 eV.

Theoretical calculations

To gain a deeper insight into the electronic structures of these boron complexes, we carried out the density functional theory (DFT) calculation at the B3LYP/6-31G(d) level. The plots of HOMOs and LUMOs and energy levels are shown in Fig. 6.

As shown in Fig. 6, the LUMOs of all complexes including the amine-substituted derivatives are the same and delocalize on the whole four-ring-fused π -conjugated skeleton. Their LUMO energy levels are very close, being in the range of -2.01 eV to -2.39 eV. These calculated results demonstrate that the electron-donating amine groups do not contribute to the LUMOs and can only slightly tune the energy levels, which is consistent with observations in the cyclic voltammetry. Replacing the bridging oxygen atom by a sulfur atom pushes the LUMO energy level down by certain degrees, which can be seen from comparisons between complexes **1** ($E_{\text{LUMO}} = -2.01$ eV) and **2** ($E_{\text{LUMO}} = -2.20$ eV) as well as **4** ($E_{\text{LUMO}} = -2.04$ eV) and **5** ($E_{\text{LUMO}} = -2.21$ eV).

In a sharp contrast, the HOMOs are quite different between non-substituted complexes (**1** and **2**) and amine-substituted derivatives (**3–6**). The molecular orbitals of **1** and **2** are delocalized on the entire ring-fused π -skeleton, whereas those of **3–6** are donated mainly by π -orbitals of the amine groups and the substituted phenyl rings. As a result, the HOMO levels of complexes **3–6** ($E_{\text{HOMO}} = -5.37$ eV for **3**, -4.98 eV for **4**, -4.98 eV for **5**, -5.13 eV for **6**) having electron-donating groups are significantly increased compared to those of complexes **1** ($E_{\text{HOMO}} = -5.87$ eV) and **2** ($E_{\text{HOMO}} = -5.86$ eV). It thus can be expected that the HOMO energy levels are dependent on the electron-donating strength of the substituted amine groups. Complex **3** exhibited a lower HOMO level compared to complexes **4**, **5**, and **6** due to the weaker electron-donating ability of the carbazole group. Modulation of the π -frame from the B, O-bridge to the B,S-bridge failed to tune the HOMO levels considering the calculated results that **1** and **2** as well as **4** and **5** respectively showed the same HOMO levels though this structural modification could tune LUMO levels by certain degrees.

Corresponding to the HOMO and LUMO levels, the energy band gaps of these complexes were determined to be 3.86 eV for **1**, 3.66 eV for **2**, 2.98 eV for **3**, 2.94 eV for **4**, 2.77 eV for **5**, and 3.02 eV for **6**. Amine derivations in **3–6** increase the HOMOs greatly but affect the LUMOs weakly; hence narrow the band gap. This result can well explain the red-shifted absorption and emission bands of **3–6**. The HOMO and LUMO distributions of amine-substituted derivatives **3–6** are donated separately by amine groups and ring-fused π -conjugated skeletons; therefore, intramolecular charge transfer (ICT) from the amine group to the core skeleton is suggested, which could partly explain their broad absorption and large Stokes shifts.

Solvatochromic behaviours

The solvatochromic behaviours were evaluated to gain insight into the ICT character of complexes **1–6**. The non-substituted

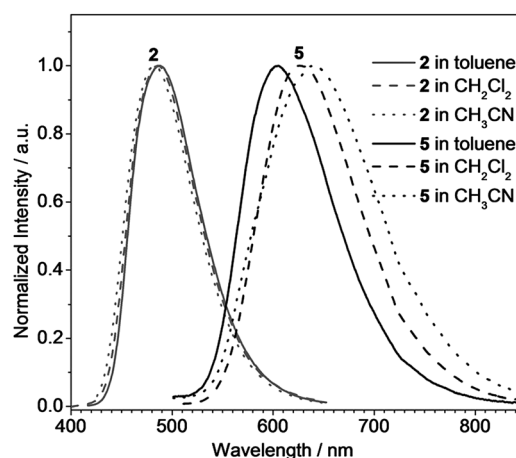


Fig. 7 Solvatochromic behaviours of complexes **2** (gray line) and **5** (black line).

complexes **1** and **2** keep an identical emission profile when the solvent polarity is increased from toluene to dichloromethane and finally to acetonitrile, whereas amine-substituted derivatives **3–6** produce gradually red-shifted emission bands after changing the solvents in the same order. The normalized emission spectra of complexes **2** and **5** in solvents of varying polarity are shown in Fig. 7 as examples and those of other four complexes are summarized in the supporting information (Fig. S3†). The emission maxima of all complexes in different solvents are collected in Table 3. The emission bands of **2** were independent of the solvent polarity. In contrast, complex **5** showed strong solvent-polarity dependent emission spectra. When the polarity of solvents increased from weak (toluene) to strong (acetonitrile), the emission band underwent remarkable bathochromic shifts while only a subtle change was observed in the absorption spectra. The degree of bathochromic shift in the fluorescence of complex **3** (20 nm) is smaller compared to those of complexes **4** (40 nm), **5** (37 nm), and **6** (40 nm), which is due to the relatively weak electron-donating ability of the carbazole group in the series of carbazole, diphenylamine, and dimethylamine.

Thermal properties

The thermal properties of **1–6** were characterized by thermogravimetric analysis (TGA) and differential scanning calorimetry (DSC) under a nitrogen atmosphere at a heating rate of 10 °C min^{-1} . The resultant data, including melting point (T_m), glass-transition temperature (T_g) from the re-melt (second heating

Table 3 Emission maxima of complexes **1–6** in different solvents^a

Complex	$\lambda_{\text{em}}/\text{nm}$ (in toluene)	$\lambda_{\text{em}}/\text{nm}$ (in CH_2Cl_2)	$\lambda_{\text{em}}/\text{nm}$ in CH_3CN
1	455	452	450
2	487	486	482
3	533	543	553
4	554	574	594
5	604	627	641
6	630	642	670

^a Concentration: 1.0×10^{-4} M.

process), and decomposition temperatures (T_{d5}), are shown in Table 2. Complexes **1** and **2** show relatively low glass-transition temperatures and melting points with T_g at 60 °C and 75 °C and T_m at 160 °C and 211 °C, respectively, due to their low molecular weight. All the amine-substituted derivatives have high glass-transition temperatures with T_g over 100 °C (142 °C for **3**, 105 °C for **4**, 115 °C for **5**, 129 °C for **6**). The melting points for **3** and **6** are 303 and 269 °C, respectively, which are much higher than that of **2**. Notably, complexes **4** and **5** do not show endothermic peaks corresponding to their melt, which is indicative of the unique glassy state of these two complexes. Among the amine-substituted derivatives, complex **3** with a carbazole group shows the highest T_g and T_m in the DSC measurement. This is probably because of the high rotation barrier of the carbazole group in **3** compared with the substituted diphenylamine and dimethylamine groups in **4**, **5**, and **6**. As determined by TGA characterization, the decomposition temperatures of amine-substituted derivatives **3–6** are 355, 324, 315, 306 °C, respectively, which are significantly higher than those of the non-substituted parent complexes **1** (238 °C) and **2** (264 °C). High-temperature resistance is a desired feature of OLED materials because of the inevitable joule heating under the device operating conditions. The increased T_g , T_m , and T_{d5} values of **3–6** make these complexes thermally robust materials.

Electroluminescent properties

To evaluate the EL properties, OLEDs with the architecture of [ITO/NPB (35 nm)/boron complexes (**3**, **4** and **6**) (25 nm)/Alq₃ (40 nm)/LiF (0.5 nm)/Al] and [ITO/NPB (35 nm)/**5** (25 nm)/TPBi (5 nm)/Bebq₂ (35 nm)/LiF (0.5 nm)/Al] were fabricated, where NPB, boron complex, and Alq₃/Bebq₂ served as a hole-transporting material, a light emitter, and an electron-transporting material, respectively, and TPBi served as a hole-blocking layer. For comparison purposes, the thickness of the hole-transporting layer, emitting layer, and electron-transporting layer are the same for all the devices, being 35 nm, 25 nm, and 40 nm, respectively. As for complex **5**, the EL spectrum of the device comprises the emission profile of Alq₃ when this device employed Alq₃ as the electron-transporting layer. Thus, we selected TPBi/Bebq₂ as electron-transporting materials in which TPBi can effectively block hole injection into the electron-transporting layer. The devices with the configuration of [ITO/NPB (20 nm)/BA (15 nm)/**1** or **2** (25 nm)/Alq₃ (40 nm)/LiF (0.5 nm)/Al] based on complexes **1** and **2** whose EL properties have not reported previously were also fabricated, in which BA¹⁶ served as an additional hole-transporting buffer layer for the purpose of hindering the formation of an exciplex between NPB and the boron complexes. As shown in Fig. 8a, the electroluminescence (EL) spectra of **1–6** show emission peaks at 465, 500, 544, 560, 612, and 652 nm, respectively, which generally correspond well with the solid emission spectra in each case; that is, the emission originates from the boron emitter. The CIE coordinates (X , Y) of these devices are (0.16, 0.19), (0.19, 0.44), (0.41, 0.55), (0.45, 0.53), (0.61, 0.39), and (0.66, 0.34), respectively, which locate in the blue, greenish blue, green, yellow, red, and deep red regions, as depicted in Fig. 8b. Notably, all the EL spectra are voltage-independent and there is little or no variation in the CIE coordinates with different voltages (Fig. 9). Thus, stable and tunable

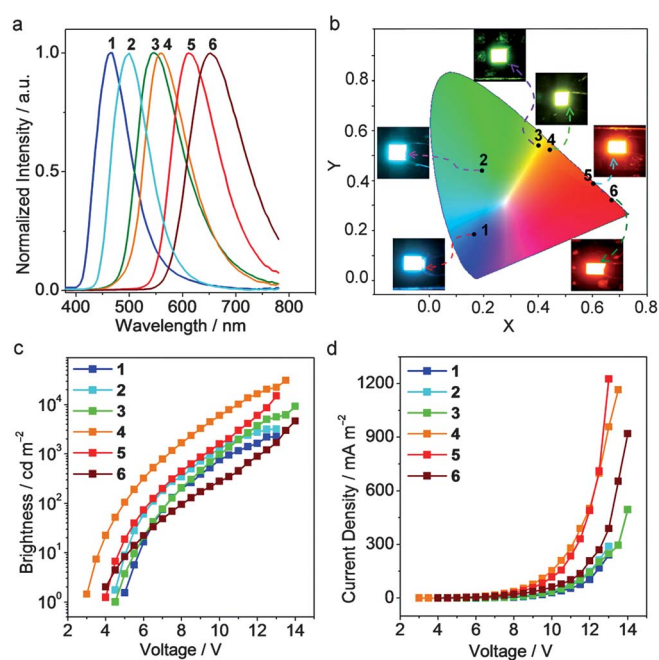


Fig. 8 Electroluminescent spectra (a), CIE coordinates and photographic images of devices employing complexes **1–6** as emitters (b), brightness–voltage (c) and current density–voltage (d) characteristics of the devices.

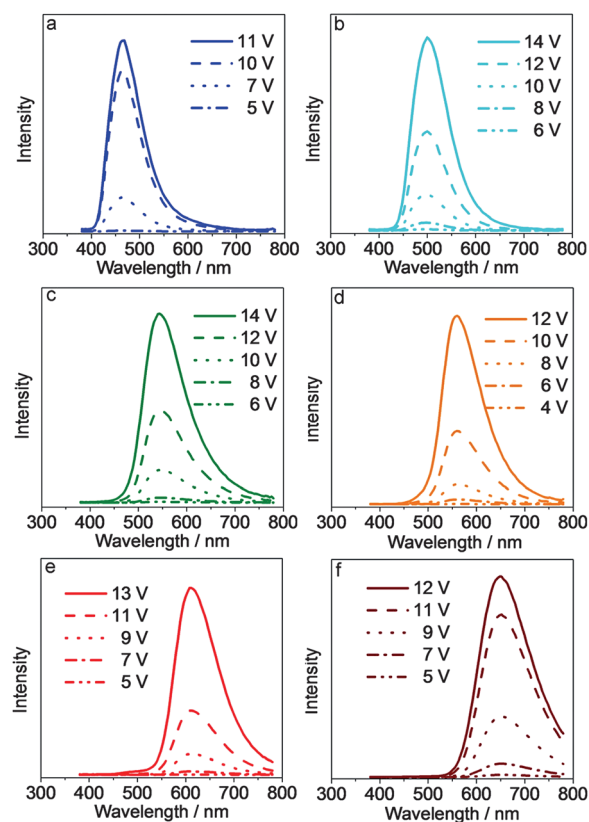


Fig. 9 EL spectra of **1** (a), **2** (b), **3** (c), **4** (d), **5** (e), and **6** (f) at different applied voltages.

Table 4 EL performance of devices employing boron complexes **1–6** as emitters

Emitter	$\lambda_{\text{EL}}^a/\text{nm}$	V_{on}^b/V	$L_{\text{max}}^c/\text{cd m}^{-2}$	$\eta_{\text{c}}^d/\text{cd A}^{-1}$	$\eta_{\text{p}}^e/\text{lm W}^{-1}$	CIE (X, Y)
1	465	5.0	2237	4.4	2.6	(0.16, 0.19)
2	500	4.8	3639	7.8	4.4	(0.19, 0.44)
3	544	4.5	9181	3.1	1.8	(0.41, 0.55)
4	560	3.0	31 220	5.5	4.8	(0.45, 0.53)
5	612	4.5	14 010	4.5	3.1	(0.61, 0.39)
6	652	4.0	4662	0.59	0.47	(0.66, 0.34)

^a Peak electroluminescence. ^b Turn-on voltage. ^c Maximum brightness. ^d Maximum current efficiency. ^e Maximum power efficiency.

EL colors ranging from blue to deep red have been realized by employing the present boron complexes as emitting materials.

The J - V and L - V characteristics of these devices are shown in Fig. 8c and d and their performance is listed in Table 4. The blue/greenish-blue emitting devices exhibited a maximum brightness, a turn-on voltage, and a peak current efficiency of 2237 cd m^{-2} , 5.0 V, and 4.4 cd A^{-1} for **1** and 3639 cd m^{-2} , 4.8 V, and 7.8 cd A^{-1} for **2**. The efficiencies are much higher than those previously reported boron-contained blue or greenish-blue light-emitting OLEDs.^{7d,8a} Devices employing **3**, **4**, **5** as emitters reached the maximum brightness of 9181, 31 220, and 14 010 cd m^{-2} , turn on voltage of 4.5, 3.0, and 4.5 V, and peak current efficiency of 3.1, 5.5, 4.5 cd A^{-1} , respectively. The brightness of devices fabricated from complex **3**, **4**, and **5** is significantly improved compared to that of **1** and **2**. From the cyclic voltammetry measurements, the HOMO levels of **3**, **4**, and **5** are estimated to be at -5.53 eV, -5.20 eV, and -5.17 eV, respectively, similar to that of the hole-transporting material NPB (-5.40 eV). Thus, the presence of amine groups has a favorable effect in hole-injecting or -transporting, and thereby improves the luminance. Notably, the efficiency of the device based on **2** and the brightness of the device based on **4** are the highest values among boron-containing emitting materials reported so far. It is also worth noting that the EL performance of the non-doped red-emitting device based on **5** is comparable to that of the typical red color device which employed DCJTb as a dopant.¹¹ As for **6**, the deep red emitting device showed a maximum brightness of 4662 cd m^{-2} and a current efficiency 0.59, both of which are higher than those of a rigid diboron-bridged red emitting material.^{8d}

Conclusions

In summary, a simple modification of a boron-bridged four-ring-fused core by introducing various amine groups allows the construction of highly efficient materials with emission bands covering a wide range from deep blue to saturated red. The rigid core skeleton together with bulky side phenyl groups attached to the boron atom enables all complexes to be intensely emissive in the solid state. Thus, the selected fluorescent core satisfied the most important issues for fluorescent materials, *i.e.*, flexibility in structural modification for color-tuning fluorescence and high solid-state quantum yield. Importantly, OLEDs employing these boron complexes as emitters not only retain the full-color tunable emission feature but also show very high EL performance.

Acknowledgements

This work was supported by the National Natural Science Foundation of China (50903037, 50733002, and 51173067), the Major State Basic Research Development Program (2009CB623600).

Notes and references

- (a) Y. Kim, J. Bouffard, S. E. Kooi and T. M. Swager, *J. Am. Chem. Soc.*, 2005, **127**, 13726; (b) A. Wakamiya, K. Mori and S. Yamaguchi, *Angew. Chem., Int. Ed.*, 2007, **46**, 4273; (c) S. Ye, J. Chen, C. Di, Y. Liu, K. Lu, W. Wu, C. Du, Y. Liu, Z. Shuai and G. Yu, *J. Mater. Chem.*, 2010, **20**, 3186; (d) B.-J. Jung, C.-B. Yoon, H.-K. Shim, L.-M. Do and T. Zyung, *Adv. Funct. Mater.*, 2001, **11**, 430.
- (a) R. Pohl, V. A. Montes, J. Shinar and P. Anzenbacher Jr, *J. Org. Chem.*, 2004, **69**, 1723; (b) A. Cirpan, L. Ding and F. E. Karasz, *Polymer*, 2005, **46**, 811.
- (a) Y.-S. Yao, Q.-Z. Zhou, X.-S. Wang, Y. Wang and B.-W. Zhang, *J. Mater. Chem.*, 2006, **16**, 3512; (b) S. A. Odom, S. R. Parkin and J. E. Anthony, *Org. Lett.*, 2003, **5**, 4245; (c) Y.-S. Yao, Q.-X. Zhou, X.-S. Wang, Y. Wang and B.-W. Zhang, *Adv. Funct. Mater.*, 2007, **17**, 93; (d) B.-J. Jung, C.-B. Yoon, H.-K. Shim, L.-M. Do and T. Zyung, *Adv. Funct. Mater.*, 2001, **11**, 430.
- (a) A. Craft, A. C. Grimsdale and A. B. Holmes, *Angew. Chem., Int. Ed.*, 1998, **37**, 402; (b) M. D. Watson, A. Fechtenkötter and K. Müllen, *Chem. Rev.*, 2001, **101**, 1267; (c) J. E. Anthony, *Angew. Chem., Int. Ed.*, 2008, **47**, 452; (d) U. Scherf, *J. Mater. Chem.*, 1999, **9**, 1853.
- (a) S. Yamaguchi, C. Xu and K. Tamao, *J. Am. Chem. Soc.*, 2003, **125**, 13662; (b) C. Xu, A. Wakamiya and S. Yamaguchi, *J. Am. Chem. Soc.*, 2005, **127**, 1638; (c) A. Fukazawa, H. Yamada and S. Yamaguchi, *Angew. Chem., Int. Ed.*, 2008, **47**, 5582; (d) H. Tian, Y. Deng, F. Pan, L. Huang, D. Yan, Y. Geng and F. Wang, *J. Mater. Chem.*, 2010, **20**, 7998; (e) R. K. Cheedarala, G.-H. Kim, S. Cho, J. Lee, J. Y. Kim and C. Yang, *J. Mater. Chem.*, 2011, **21**, 843.
- (a) Q. Wu, M. Esteghamatian, N.-X. Hu, Z. Popovic, G. Enright, Y. Tao, M. Diorio and S. Wang, *Chem. Mater.*, 2000, **12**, 79; (b) Q. Liu, M. S. Mudadu, H. Schmider, R. Thummel, Y. Tao and S. Wang, *Organometallics*, 2002, **21**, 4743; (c) Y. Cui, Q.-D. Liu, D.-R. Bai, W.-L. Jia, Y. Tao and S. Wang, *Inorg. Chem.*, 2005, **44**, 601; (d) Q.-D. Liu, M. S. Mudadu, R. Thummel, Y. Tao and S. Wang, *Adv. Funct. Mater.*, 2005, **15**, 143.
- (a) Y. Li, Y. Liu, W. Bu, J. Guo and Y. Wang, *Chem. Commun.*, 2000, 1551; (b) J. Feng, F. Li, W. B. Gao, S. Y. Liu, Y. Liu and Y. Wang, *Appl. Phys. Lett.*, 2001, **78**, 3479; (c) Y. Liu, J. Guo, H. Zhang and Y. Wang, *Angew. Chem., Int. Ed.*, 2002, **41**, 182; (d) H. Zhang, C. Huo, K. Ye, P. Zhang, W. Tian and Y. Wang, *Inorg. Chem.*, 2006, **45**, 2788; (e) H. Zhang, C. Huo, J. Zhang, P. Zhang, W. Tian and Y. Wang, *Chem. Commun.*, 2006, 281.
- (a) Z. L. Zhang, H. Bi, Y. Zhang, D. D. Yao, H. Z. Gao, Y. Fan, H. Y. Zhang, Y. Wang, Y. P. Wang, Z. Y. Chen and D. G. Ma, *Inorg. Chem.*, 2009, **48**, 7230; (b) D. Li, Z. Zhang, S. Zhao, Y. Wang and H. Zhang, *Dalton Trans.*, 2011, **40**, 1279; (c) D. Li, Y. Yuan, H. Bi, D. D. Yao, X. J. Zhao, W. J. Tian, Y. Wang and H. Y. Zhang, *Inorg. Chem.*, 2011, **50**, 4825; (d) D. Li, K. Wang,

- S. Huang, S. N. Qu, X. Y. Liu, Q. X. Zhu, H. Y. Zhang and Y. Wang, *J. Mater. Chem.*, 2011, **21**, 15298.
- 9 M. J. Kwak and Y. Kim, *Bull. Korean Chem. Soc.*, 2009, **30**, 2865.
- 10 D. Yao, S. Zhao, J. Guo, Z. Zhang, H. Zhang, Y. Liu and Y. Wang, *J. Mater. Chem.*, 2011, **21**, 3568.
- 11 T. W. Lee, O. O. Park, H. N. Cho and Y. C. Kim, *Curr. Appl. Phys.*, 2001, **363**, 1.
- 12 *SHELXTL, Version 5.1*; Siemens Industrial Automation, Inc. 1997; G. M. Sheldrick, *SHELXS-97, Program for Crystal Structure Solution*; University of Göttingen: Göttingen, 1997.
- 13 E. Runge and E. K. U. Gross, *Phys. Rev. Lett.*, 1984, **52**, 997.
- 14 A. D. J. Becke, *Chem. Phys.*, 1993, **98**, 5648.
- 15 M. J. Frisch, G. W. Trucks, H. B. Schlegel, G. E. Scuseria, M. A. Robb, J. R. Cheeseman, J. A. Montgomery Jr., T. Vreven, K. N. Kudin, J. C. Burant, J. M. Millam, S. S. Iyengar, J. Tomasi, V. Barone, B. Mennucci, M. Cossi, G. Scalmani, N. Rega, G. A. Petersson, H. Nakatsuji, M. Hada, M. Ehara, K. Toyota, R. Fukuda, J. Hasegawa, M. Ishida, T. Nakajima, Y. Honda, O. Kitao, H. Nakai, M. Klene, X. Li, J. E. Knox, H. P. Hratchian, J. B. Cross, C. Adamo, J. Jaramillo, R. Gomperts, R. E. Stratmann, O. Yazyev, A. J. Austin, R. Cammi, C. Pomelli, J. W. Ochterski, P. Y. Ayala, K. Morokuma, G. A. Voth, P. Salvador, J. J. Dannenberg, V. G. Zakrzewski, S. Dapprich, A. D. Daniels, M. C. Strain, O. Farkas, D. K. Malick, A. D. Rabuck, K. Raghavachari, J. B. Foresman, J. V. Ortiz, Q. Cui, A. G. Baboul, S. Clifford, J. Cioslowski, B. B. Stefanov, G. Liu, A. Liashenko, P. Piskorz, I. Komaromi, R. L. Martin, D. J. Fox, T. Keith, M. A. Al-Laham, C. Y. Peng, A. Nanayakkara, M. Challacombe, P. M. W. Gill, B. Johnson, W. Chen, M. W. Wong, C. Gonzalez, J. A. Pople, *Gaussian 03, Revision C.02*, Gaussian, Inc.: Pittsburgh, PA 2003.
- 16 Y. Yuan, D. Li, X. Zhang, X. Zhao, Y. Liu, J. Zhang and Y. Wang, *New J. Chem.*, 2011, **35**, 1534.